

Article

Control-Oriented Electrochemical Model and Parameter Estimation for an All-Copper Redox Flow Battery

Wouter Badenhorst ^{1,†}, Christian M. Jensen ^{2,†}, Uffe Jakobsen ², Zahra Esfahani ² and Lasse Murtomäki ^{1,*}

¹ Department of Chemistry and Materials Science, School of Chemical Engineering, Aalto University, 02150 Espoo, Finland; wouter.badenhorst@aalto.fi

² Department of Electrical and Computer Engineering, Aarhus University, 8000 Aarhus, Denmark; cmje@ece.au.dk (C.M.J.); uja@ece.au.dk (U.J.); z.esf@ece.au.dk (Z.E.)

* Correspondence: lasse.murtomaki@aalto.fi

† These authors contributed equally to this work.

Abstract: Redox flow batteries are an emergent technology in the field of energy storage for power grids with high renewable generator penetration. The copper redox flow battery (CuRFB) could play a significant role in the future of electrochemical energy storage systems due to the numerous advantages of its all-copper chemistry. Furthermore, like the more mature vanadium RFB technology, CuRFBs have the ability to independently scale power and capacity while displaying very fast response times that make the technology attractive for a variety of grid-supporting applications. As with most batteries, the efficient operation of a CuRFB is dependent on high-quality control of both the charging and discharging process. In RFBs, this is typically complicated by highly nonlinear behaviour, particularly at either extreme of the state of charge. Therefore, the focus of this paper is the development and validation of a first-principle, control-appropriate model of the CuRFBs electrochemistry that includes the impact of the flow, charging current, and capacity fading due to diffusion and subsequent comproportionation. Parameters for the proposed model are identified using a genetic algorithm, and the proposed model is validated along with its identified parameters using data obtained from a single-cell CuRFB flow battery as well as a simpler diffusion cell design. The proposed model yields good qualitative fits to experimental data and physically plausible concentration estimates and appears able to quantify the long-term state of health due to changes in the diffusion coefficient.

Keywords: all-copper redox flow battery; electrochemical model; genetic algorithm; energy storage; state of charge; control-appropriate model



Citation: Badenhorst, W.; Jensen, C.M.; Jakobsen, U.; Esfahani, Z.; Murtomäki, L. Control-Oriented Electrochemical Model and Parameter Estimation for an All-Copper Redox Flow Battery. *Batteries* **2023**, *9*, 272. <https://doi.org/10.3390/batteries9050272>

Academic Editor: Sylvain Franger

Received: 7 April 2023

Revised: 8 May 2023

Accepted: 11 May 2023

Published: 15 May 2023



Copyright: © 2023 by the authors. Licensee MDPI, Basel, Switzerland. This article is an open access article distributed under the terms and conditions of the Creative Commons Attribution (CC BY) license (<https://creativecommons.org/licenses/by/4.0/>).

1. Introduction

Energy storage system (ESS) technology has been rapidly advancing in the last twenty years [1–3] due to its potential key role in the decarbonisation of the energy mix through providing relevant grid services which assist in the integration of renewable energy generators. Recently, there has been a shift towards accelerating the adoption of renewable energy sources in all major markets, to move away from fossil fuel-based energy sources and diversify the energy mix. However, this large-scale adoption of renewable energy has led to a subsequent need for large-scale energy storage systems (ESSs) for renewable firming, frequency control regulation, and other grid services to assist in the integration of these new capacities. These energy storage systems should be durable, efficient, and ideally be a long-term sustainable solution.

A significant driver of large-scale ESS adoption is the integration of wind and solar power into the existing grid by addressing their intermittent nature and output variability because these systems fluctuate with environmental and time-of-day factors. In this application, an ESS stores excess energy during overproduction periods, and then discharges the stored energy during either high-demand or low-production periods. The choice of

ESS for a given application will depend on the power and energy ratings, response time requirements, weight, volume, and operating temperature of the application [4]. In addition to renewable firming, an ESS can also provide a variety of ancillary services that increase grid stability and reliability.

One of the emerging technologies in the field of ESSs is redox flow batteries (RFBs), as they have shown to be a promising solution for large-scale energy storage due to their cost-effectiveness, system flexibility, and fast response time. RFBs complement the intermittent nature of renewable energy sources, such as wind and solar, particularly well [5]. RFBs also have advantages over existing Na-ion and Li-ion ESS technology. The power and capacity rating can be decoupled, allowing the optimal power and capacity rating to be selected independently for the intended use case. RFBs also have a longer cycle life than conventional batteries. These benefits make RFBs a promising solution to the intermittent nature of renewable energy sources, helping to store excess energy during low demand and release it during peak demand, thereby improving the stability and reliability of the power grid [6–8].

According to the Department of Energy's (DOE) global energy storage database, RFBs account for approximately 18% of the installed electrochemical battery storage, 19% for Na-ion batteries and the remaining 63% for Li-ion batteries, when looking at installed capacity and only at the top three technologies in this category. Of the installed RFB capacity, vanadium RFBs account for nearly 74% of the rated power. However, despite this large current market share, the technology has concerns regarding the scarcity of vanadium that is preventing further adoption. This raw material scarcity of vanadium has led to the development of new emerging RFB technologies in an effort to move away from critical, hard-to-source raw materials. One such emerging technology is the aqueous all-copper redox flow battery, which has garnered increased attention in the last four years [9]. The primary advantages are the low-cost active material, which has high solubility, high energy efficiency, and low overall costs. Furthermore, the electrolyte is easy to manufacture and rebalance. These benefits have driven the aqueous all-copper RFB to become an attractive choice for playing a role in the integration of renewable sources, grid stabilisation, and energy storage in off-grid environments [10–12], and as such, copper redox flow batteries (CuRFBs) have the potential to become a significant player in the future of electrochemical energy storage systems.

In a recent study, the performance of the CuRFB system has been improved through optimisation of the separator choice, electrode modifications, and operation optimisations [13]. The largest improvement originates from the reduction in the self-discharge rate of the system, extending the operational time without maintenance from the previous 9 h to over 210 h [13,14]. This is achieved by slowing the transport of Cu(II) (Equation (1)), formed during the charging process in the anolyte to the catholyte where metallic copper is deposited (Equation (2)). This transport results in a comproportionation reaction (Equation (3)) between the Cu(II) and metallic copper resulting in the formation of 2Cu(I), thereby lowering the current efficiency and reducing—albeit reversibly—the maximum achievable capacity as the system becomes unbalanced. While we have a basic understanding of the underlying electrochemical behaviour of the CuRFB, the authors are not aware of any preexisting attempts to explicitly model the battery dynamics. This lack of dynamical models—and the derived lack of ability to estimate battery parameters and underlying system states—makes it difficult to achieve consistently high energy and voltage efficiency [15].

To try and address this knowledge gap, this paper focuses on the electrochemical modelling of the CuRFB to assist in further optimisation of the CuRFB. First and foremost, the purpose of this article is to propose a concentration-based model of copper concentration dynamics and cell voltage. The battery model parameters are identified from experimental data using a genetic algorithm (GA).

The remainder of this work is organised as follows. In Section 2, a dynamical model of the CuRFB is proposed based on the electrochemistry of its three aqueous species. Further-

more, this section gives an expression for the cell voltage, state of charge (SOC), and state of health (SOH) based on the modelled concentrations. In Section 3, the framework for data generation is introduced, along with the materials and methods. Then, the operating parameters and testing procedure are presented. The model parameter identification approach is presented in Section 4. The experimental results and identified model parameters are presented in Section 5. Sections 6 and 7 discuss the agreement of the identified models with experimental data and summarise the key findings of the paper, respectively.

2. CuRFB Dynamical Model

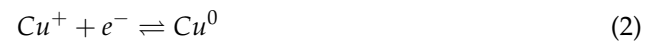
In the following section, we describe our suggested dynamical model of the CuRFB. We propose a model of copper concentration dynamics and cell voltage, as well as concentration-based state of charge (SOC) and both short-term and long-term state-of-health (SOH) metrics.

2.1. Copper Concentration Dynamics

Much like the well-understood vanadium redox flow battery (VRFB), the CuRFB relies on a reversible redox reaction. At the anode, Cu^+ oxidises during charging to form Cu^{2+} :



while at the cathode, Cu^+ is reduced during charging to form Cu^0 :



Furthermore, during operation, Cu^{2+} may migrate across the membrane and undergo disproportionation with Cu^0 to form cathode-side Cu^+ :



This reaction structure resembles the reaction structure of a VRFB to a great extent. However, while all four redox species in a VRFB are soluble and present in both the cells and tanks, Cu^0 is present as an electrodeposited solid and should not occur in the tanks under normal operating conditions. On account of this, we take a slightly different approach than common electrochemical VRFB models [16,17] and only model the soluble CuRFB species. This results in a six-state model where—with c_{1a} , c_{1c} , and c_{2a} denoting, respectively, anolyte-side Cu^+ , catholyte-side Cu^+ , and anolyte-side Cu^{2+} —the cell concentration dynamics are given by

$$\frac{d}{dt} \begin{bmatrix} c_{1a}^{cell} \\ c_{1c}^{cell} \\ c_{2a}^{cell} \end{bmatrix} = \frac{1}{V_{cell}} \left(\begin{bmatrix} c_{1a}^{tank} - c_{1a}^{cell} \\ c_{1c}^{tank} - c_{1c}^{cell} \\ c_{2a}^{tank} - c_{2a}^{cell} \end{bmatrix} Q + \frac{1}{zF} \begin{bmatrix} -1 \\ -1 \\ 1 \end{bmatrix} I + \frac{S}{d} \begin{bmatrix} 0 & 0 & 0 \\ 0 & 0 & 2D \\ 0 & 0 & -D \end{bmatrix} \begin{bmatrix} c_{1a}^{cell} \\ c_{1c}^{cell} \\ c_{2a}^{cell} \end{bmatrix} \right) \quad (4)$$

and the tank concentration dynamics are given by

$$\frac{d}{dt} \begin{bmatrix} c_{1a}^{tank} \\ c_{1c}^{tank} \\ c_{2a}^{tank} \end{bmatrix} = \frac{1}{V_{tank}} N \begin{bmatrix} c_{1a}^{cell} - c_{1a}^{tank} \\ c_{1c}^{cell} - c_{1c}^{tank} \\ c_{2a}^{cell} - c_{2a}^{tank} \end{bmatrix} Q \quad (5)$$

where V_{cell} is the cell volume, V_{tank} is the tank volume, N denotes the number of cells in the CuRFB stack, c_*^{cell} denotes the cell concentration of a species, c_*^{tank} denotes the tank concentration of a species, Q is the applied electrolyte flow rate, I is the applied current, D is the cross-membrane diffusion rate of Cu^{2+} , z is the number of electrons exchanged by the redox process, F is the Faraday constant, S is the membrane surface area, and d is the membrane thickness.

2.2. Cell Voltage

Generally, in a redox flow battery of a variety of chemistries, the cell voltage consists of a reduction potential (given by the formal potential V_0 and the Nernst equation), the activation overpotential (given by the Butler–Volmer equation), and the ohmic overpotential:

$$V_{cell} = V_0 + V_{Nernst} + V_{act} + V_{\Omega} \quad (6)$$

The Nernst term is a logarithmic function of the ratios between oxidised and reduced species in each half-cell:

$$V_{Nernst} = \frac{RT}{zF} \ln \left(\frac{c_{2a}^{cell} \cdot 1M}{c_{1a}^{cell} \cdot c_{1c}^{cell}} \right) \quad (7)$$

Note that the numerator is taken as 1 M (1000 mol/m³) in the cathode-side term as Cu^0 is solid.

The activation overpotentials are given by the Butler–Volmer equations. Under the assumption that the charge transfer coefficient α is 0.5 for both the anode and cathode, the activation overpotentials can be calculated directly [18]:

$$V_{act} = V_+ - V_- \quad (8)$$

$$V_+ = \frac{2RT}{F} \ln \left(\frac{1}{2j_+S} I + \sqrt{\left(\frac{1}{2j_+S} I \right)^2 + 1} \right) \quad (9)$$

$$V_- = \frac{2RT}{F} \ln \left(\frac{1}{2j_-S} I + \sqrt{\left(\frac{1}{2j_-S} I \right)^2 + 1} \right) \quad (10)$$

where j_+, j_- are the concentration-dependent exchange current densities which can be calculated as

$$j_+ = \frac{1}{S} \left(F \cdot k_+ \cdot (c_{2a}^{cell})^{1-\alpha} \cdot (c_{1a}^{cell})^{\alpha} \right) \quad (11)$$

$$j_- = \frac{1}{S} \left(F \cdot k_- \cdot (1M)^{1-\alpha} \cdot (c_{1c}^{cell})^{\alpha} \right) \quad (12)$$

where k_+, k_- are the rate constants of, respectively, the anolyte and catholyte; R is the ideal gas constant; and as in the Nernst equation, the Cu^0 concentration is taken as 1 M.

Under the assumption that system parameters do not change meaningfully due to degradation, the ohmic overpotential can be represented as a function of a constant resistance R_{stack} and applied current I :

$$V_{\Omega} = R_{stack} I \quad (13)$$

Finally, we propose a voltage offset term V_{off} that may differ between charging and discharging but is otherwise constant. This offset is intended to capture phenomena relating to, e.g., copper deposition, which cannot be represented by the lumped nature of the proposed model. The full voltage expression then is

$$V_{cell} = V_0 + V_{Nernst} + V_{act} + V_{\Omega} + V_{off} \quad (14)$$

2.3. State of Charge

As in other redox flow batteries, the SOC of the CuRFB can be expressed via the species ratio in the tanks. In four-species models like the ones commonly used for VRFBs [16,17], this results in two separate SOC expressions for, respectively, the anolyte and catholyte species. In the proposed model, however, Cu^+ in the anolyte circuit is always the limiting

factor due to the structure of the comproportionation reaction Equation (3), and a single unambiguous SOC metric is therefore given by the anolyte-side species ratio:

$$SOC = \frac{c_{2a}^{tank}}{c_{2a}^{tank} + c_{1a}^{tank}} \quad (15)$$

where $SOC \in [0 \dots 1]$.

2.4. Short-Term State of Health

The limiting factor for battery SOH during normal day-to-day operation is the species imbalance induced by the comproportionation reaction Equation (3), which results in an accumulation of excess Cu^+ in the catholyte circuit. This results in a short-term SOH model given by

$$SOH = \frac{c_{1a}^{tank}}{c_{1c}^{tank}} \quad (16)$$

where $SOH \in [0 \dots 1]$ and the concentrations should be measured at the start of each charging cycle.

2.5. Long-Term State of Health

The experimental results indicate that component degradation is not a significant concern on short-to-medium-term timescales but does meaningfully affect battery performance on longer timescales. In particular, as we describe in Section 5, long-term (12+ months) exposure to the electrolyte appears to alter the membrane transport properties and increase the rate at which diffusion occurs. We propose that this mode of degradation can be quantified by the following expression:

$$SOH_L = \frac{D_{nom}}{D} \quad (17)$$

where $SOH_L \in [0 \dots 1]$, D_{nom} is the nominal membrane diffusion coefficient, D is the current membrane diffusion coefficient, and we assume D is strictly decreasing as a function of time.

3. Materials and Methods

The data for the model parameter estimation and fitting were obtained from both a small-scale diffusion cell and a larger single-cell flow battery. Both of these systems were operated with 1 M CuCl and 6 M HCl as the electrolytes, and for both, the cut-off voltages were set to 0.9 and 0.3 V for charge and discharge, respectively. In the case of the diffusion cell, 20 mA was applied and 0.5 A for the single-cell flow battery, resulting in a current density of 20 mA/cm² for both test cases. The equipment, experimental procedure, and electrolyte preparation methods were performed as previously reported [13], and the FAP-330 anion exchange membrane obtained from FUMATECH BWT GmbH was used. In addition to this, extra experiments were performed on the FAP-330 sample originally used in 2021 and published in 2022 [13], during which it was operated for 1200 h (300 cycles) and then left in a solution of 1 M CuCl and 6 M HCl for over one and a half years before being retested in this paper. The experimental setups used are shown in Figure 1.

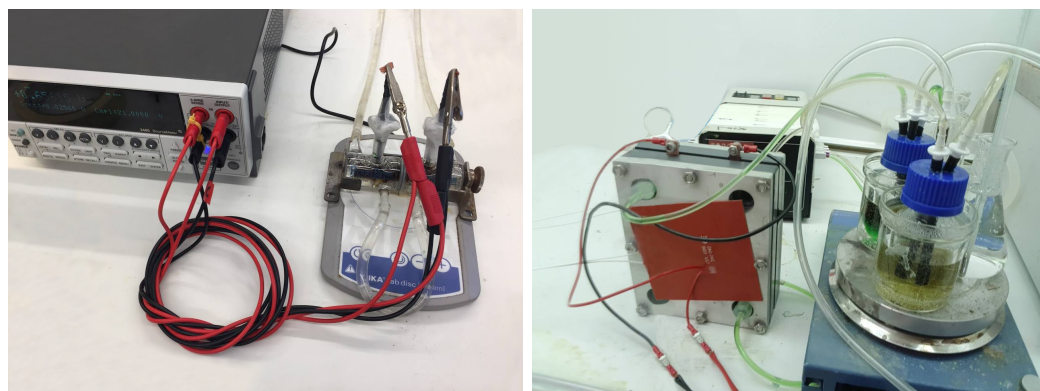


Figure 1. Experimental setups used in this study for validation of the proposed electrochemical model and parameter estimation. (a) Diffusion cell (1 cm²). (b) Single cell (25 cm²).

4. Genetic Algorithm

To estimate parameters, a simple genetic algorithm (GA) is used. A GA is here defined as a biologically inspired evolutionary method, where a randomly initialised population of parameter estimates evolves based on a set of operations applied to several generations of the population.

For some problems, a GA compares favourably with gradient-based methods [19]. The presented GA uses a direct floating point representation of the parameter estimates, and operators such as mutation and crossover operate directly on the floating point values. This simplifies and speeds up implementation [20,21]. The basic algorithm is shown in Figure 2.

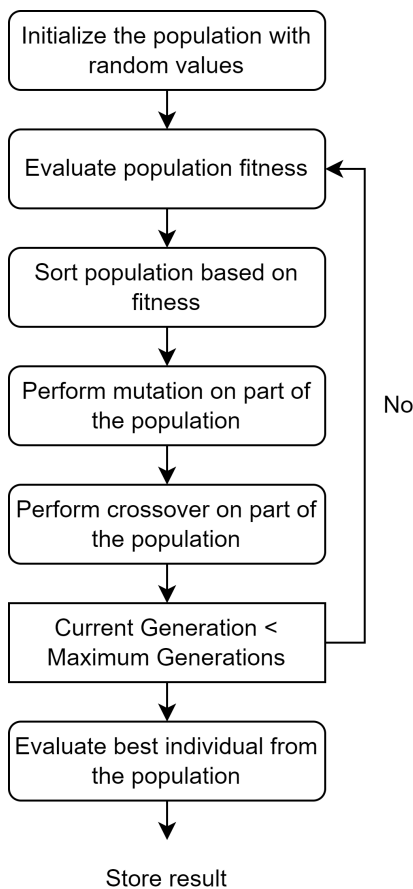


Figure 2. UML activity chart of the used genetic algorithm.

The population consists of a fixed number of individuals in an array. Each individual has a fixed number of parameters. The GA implementation has an elite subpopulation of individuals that are exempt from crossover and mutation. Another subpopulation is only exposed to crossover, and the last part of the population experiences both crossover and mutation.

Fitness is evaluated by having the recorded current and flow as input to the battery model. The battery model calculates the voltage estimate ($V_{model}(t)$) corresponding to each time-step of the recorded data and this is evaluated against the recorded voltage ($V_{measured}(t)$) to calculate fitness ($item_{fit}$), as seen in Equation (18).

$$item_{fit} = \int_{T_1}^{T_2} (V_{measured}(t) - V_{model}(t))^2 dt \tag{18}$$

where T_1 is the start of the recorded current/voltage and T_2 is the end. As seen from Equation (18), a small value indicates good fitness. The integral is implemented as a forward Euler integration in the program.

Crossover method: Given two individuals ($item_1$ (from the elite population) and $item_2$ (from the entire population)) selected for crossover, for each parameter called $item_{1_{par}}$ and $item_{2_{par}}$ with fitness $item_{1_{fit}}$ and $item_{2_{fit}}$, respectively, the crossover is performed and is stored in a new parameter $item_{new_{par}}$ as described in Equation (19).

$$item_{new_{par}} = \frac{item_{1_{par}} \cdot item_{1_{fit}} + item_{2_{par}} \cdot item_{2_{fit}}}{item_{1_{fit}} + item_{2_{fit}}} \tag{19}$$

Mutation method: Given an individual ($item_1$) selected for mutation, each parameter for the individual is called $item_{1_{par}}$. A pseudo-random generator ($random()$) is used to generate numbers in the range of $[0; 1]$. The mutation is controlled by the following parameters:

mut_{rate} : Rate of mutations.

mut_{int} : Mutation intensity.

$current_{gen}$: Current generation number. Inspired by simulated annealing as described in [22], the mutation intensity is decreased each generation (see Equations (20) and (21)).

max_{gen} : Maximum allowed number of generations.

$parameter_{max}$: Maximum allowed value for a given parameter.

$parameter_{min}$: Minimum allowed value for a given parameter.

$\Delta_{par} = parameter_{maximum} - parameter_{minimum}$

A helper function $random_{limited}(minimum, maximum)$ calculates a random value between $minimum$ and $maximum$.

$$noise = \begin{cases} \left(1 - \frac{current_{gen}}{max_{gen}}\right) \cdot mut_{int} \cdot \Delta_{par}, & \text{if } random() < mut_{rate} \\ 0, & \text{otherwise} \end{cases} \tag{20}$$

$$item_{new_{par}} = random_{limited}(item_{1_{par}} - noise, item_{1_{par}} + noise) \tag{21}$$

As a final step, the best individual from the last generation is evaluated and run and the simulation result is stored, so an offline comparison of the result can be made. The full GA algorithm developed as part of this paper is written in Rust and is publicly available [23].

5. Experimental Verification

The proposed model was validated using the single-cell and diffusion-cell experimental setups described in Section 3. The genetic algorithm described in Section 4 was used to identify the model parameters in both cases. We first present the validation results from the single-cell setup, and then present the results from the two experimental datasets obtained with the diffusion cell, with the latter dataset being used to quantify membrane degradation through tracking the diffusion number after 300+ cycles of operation and 18 months of continuous electrolyte exposure.

5.1. Single Cell

Only a single charge–discharge cycle was used to fit the single-cell parameters due to the clear presence of non-standard behaviour in the first two cycles seen in Figure 3. We presume the first cycle behaviour is due to limited chloride availability as reported in [13], while the drastic capacity loss from cycles 2 to 3 may be due to copper delamination.

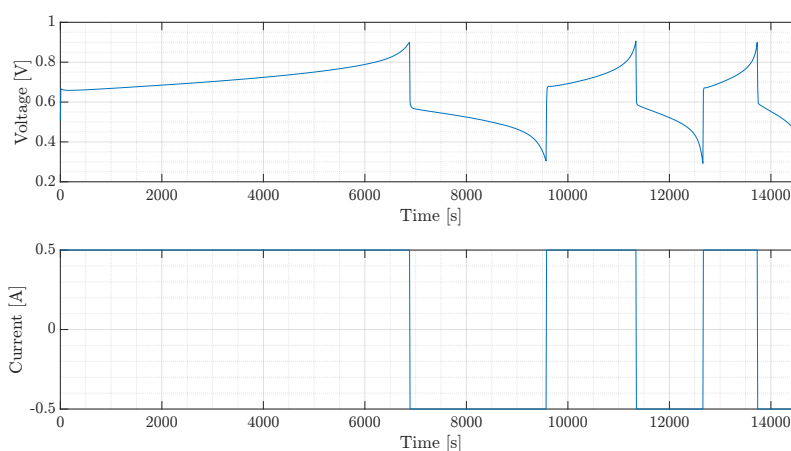


Figure 3. Charge and discharge voltages for 3 cycles with the single cell.

We fit the parameters in Table 1 using the genetic algorithm described in Section 4. The data were downsampled to a sampling rate of $T_s = 10$ s, and the proposed dynamical model of the CuRFB was discretised using the forward Euler method. The obtained membrane diffusion numbers, Ref. [24], and reaction rate constants align with previously reported values [25].

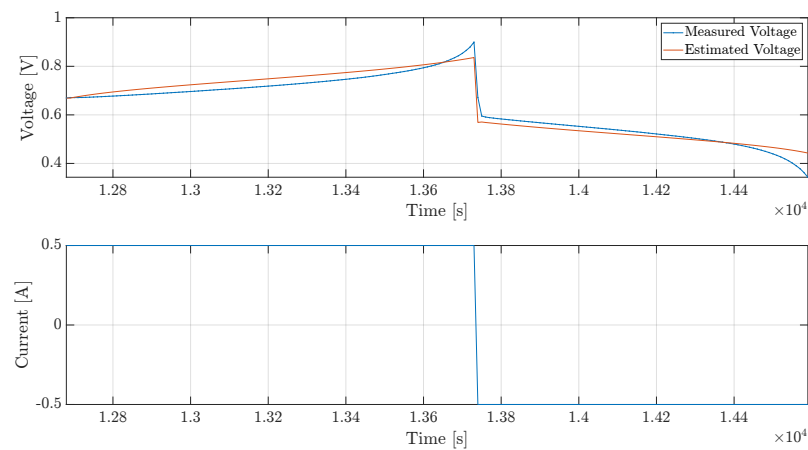
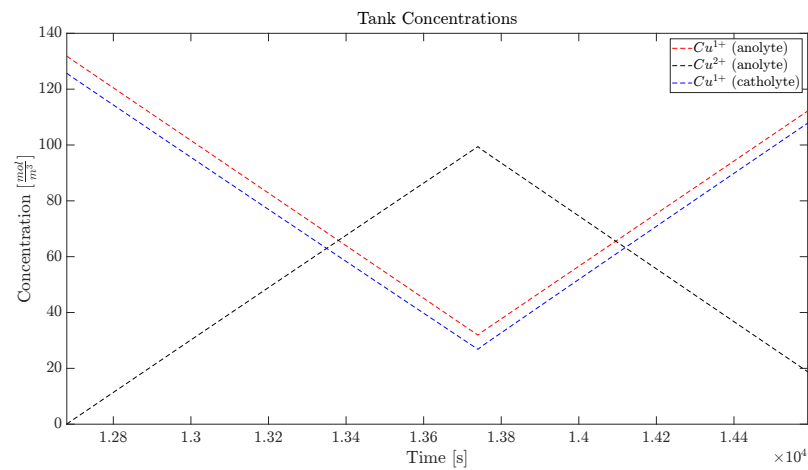
Table 1. Identified model parameters, single cell.

| Parameter | Value (Single Cell) |
|-----------------------|---|
| c_{1a} | 131 mol/m ³ |
| c_{1c} | 125 mol/m ³ |
| R_{stack} | 1.63 Ω |
| k_+ | $8.3 \cdot 10^{-1}$ ms ⁻¹ |
| k_- | $7.6 \cdot 10^{-5}$ ms ⁻¹ |
| D | $6.3 \cdot 10^{-12}$ m ² s ⁻¹ |
| V_{off} (charge) | -0.788 V |
| V_{off} (discharge) | 0.620 V |

The parameter bounds can be seen in Table 2. Figure 4 shows the estimated voltages from the single-cycle model compared to a single cycle of measurements, while Figure 5 shows the corresponding estimated tank concentrations.

Table 2. Model Parameter Bounds.

| Parameter | Bounds |
|-----------------------|---|
| c_{1a} | $[0, 1200]$ mol/m ³ |
| c_{1c} | $[0, 1200]$ mol/m ³ |
| R_{stack} | $[0, 5.0]$ Ω |
| k_+ | $[1 \cdot 10^{-4}, 1.0]$ ms ⁻¹ |
| k_- | $[1 \cdot 10^{-4}, 1 \cdot 10^{-7}]$ ms ⁻¹ |
| D | $[1 \cdot 10^{-11}, 1 \cdot 10^{-13}]$ m ² s ⁻¹ |
| V_{off} (charge) | $[0, 1.0]$ V |
| V_{off} (discharge) | $[0, 1.0]$ V |

**Figure 4.** Comparison of measured and estimated voltage from the single cell, 1 cycle.**Figure 5.** Estimated concentrations from the single cell, 1 cycle.

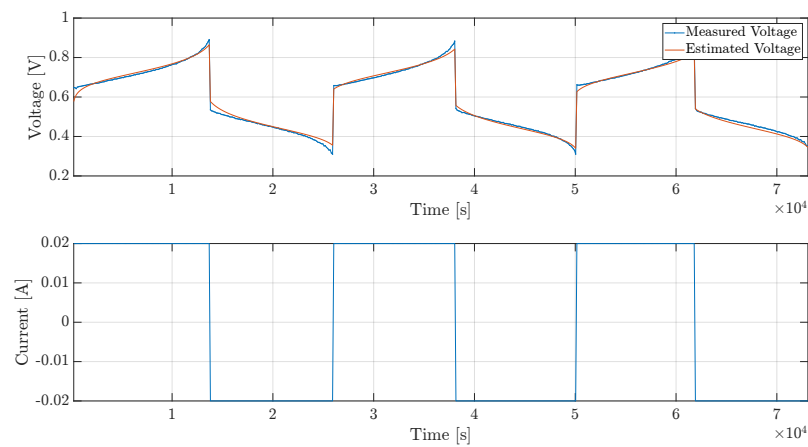
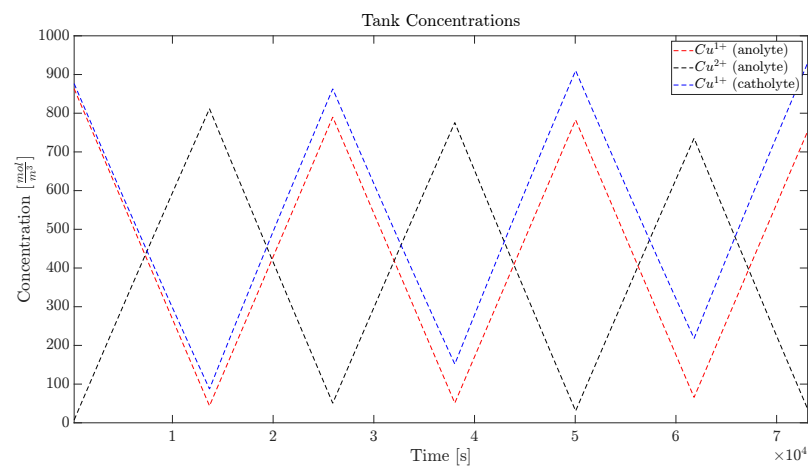
5.2. Diffusion Cell

Two sets of model parameters were identified using the respective data originally reported in [13] and the data obtained from the same membrane aged for 18 months in the CuRFB electrolyte. The data were downsampled to a sampling rate of 2 min to accommodate the much longer cycling time of the diffusion cell. Furthermore, to accommodate the lack of tanks in the diffusion cell, we assumed $c_{cell} = c_{tank}$ at all times, effectively eliminating the impact of cell/tank concentration gradients on the model.

We used the same model parameter bounds as in Table 2 and obtained the parameters seen in Tables 3 and 4. The obtained voltage and concentration trajectories can be seen in Figures 6–9.

Table 3. Identified model parameters, diffusion cell.

| Parameter | Value (Diffusion Cell) |
|-----------------------|---|
| c_{1a} | 870 mol/m ³ |
| c_{1c} | 883 mol/m ³ |
| R_{stack} | 1.4 Ω |
| k_+ | $6.7 \cdot 10^{-1}$ ms ⁻¹ |
| k_- | $7.3 \cdot 10^{-5}$ ms ⁻¹ |
| D | $3.1 \cdot 10^{-12}$ m ² s ⁻¹ |
| V_{off} (charge) | 0.032 V |
| V_{off} (discharge) | -0.191 V |

**Figure 6.** Comparison of measured and estimated voltage with diffusion cell, 3 cycles.**Figure 7.** Estimated concentrations from the diffusion cell, 3 cycles.**Table 4.** Identified model parameters, aged diffusion cell.

| Parameter | Value (Aged Diffusion Cell) |
|-----------------------|---|
| c_{1a} | 919 mol/m ³ |
| c_{1c} | 807 mol/m ³ |
| R_{stack} | 1.47 Ω |
| k_+ | $3.9 \cdot 10^{-1}$ ms ⁻¹ |
| k_- | $4.7 \cdot 10^{-5}$ ms ⁻¹ |
| D | $7.4 \cdot 10^{-12}$ m ² s ⁻¹ |
| V_{off} (charge) | 0.028 V |
| V_{off} (discharge) | -0.162 V |

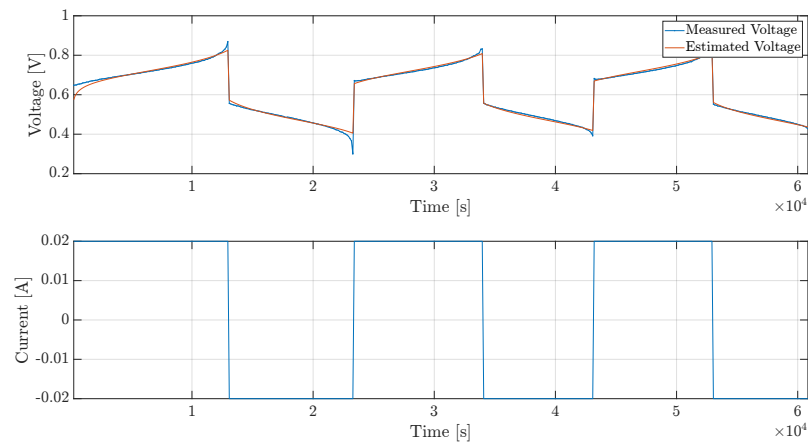


Figure 8. Comparison of measured and estimated voltage, diffusion cell.

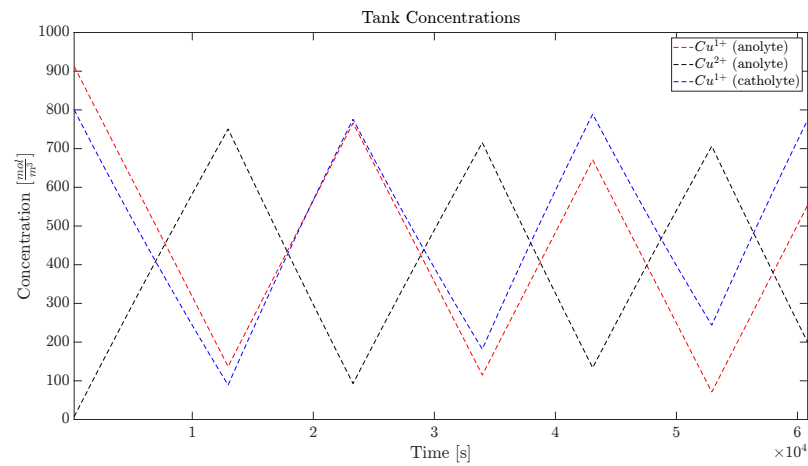


Figure 9. Estimated concentrations, diffusion cell.

5.3. Diffusion Cell, Long Trajectory

As a final point of interest, we show the results from a model fit to four full days worth of diffusion cell cycling data. We report this primarily to demonstrate the shortcomings of the proposed model over long time horizons and therefore do not report the parameter estimates, although we note that these are generally in line with the parameters found in Tables 3 and 4. The fitted voltage can be seen in Figure 10, with the corresponding concentration trajectories in Figure 11.

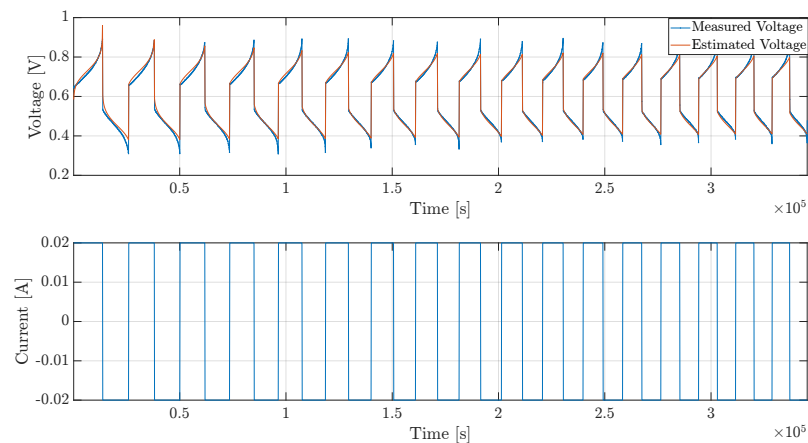


Figure 10. Comparison of measured and estimated voltage, diffusion cell, long trajectory.

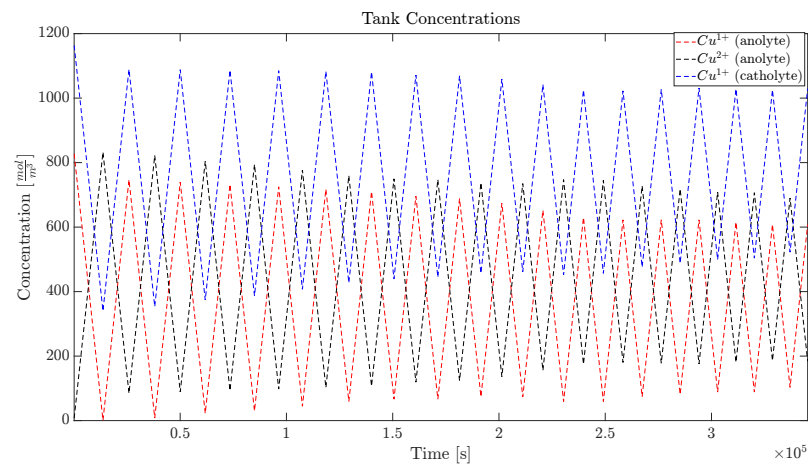


Figure 11. Estimated concentration trajectories, diffusion cell, long trajectory

6. Discussion

As can be seen from the figures presented in Section 5, the proposed model reproduces real voltage trajectories from both the regular and aged diffusion cell with excellent accuracy over short timescales while struggling to a greater extent to replicate the single-cell data and the diffusion cell behaviour on longer timescales.

With respect to the single-cell data, the obtained model is clearly not a good qualitative fit. In particular, the slope of the estimated voltage curve does not follow the true voltage curve during charge or discharge, suggesting that the underlying concentrations do not reach the appropriate extremes at the ends of these cycles. This is confirmed when the concentration trajectories are examined, where the estimated concentrations are both inappropriately low relative to the known molarity of the prepared electrolyte, and the concentrations never approach values that could reasonably be considered full charge or discharge. This is further exacerbated by the current model not being able to account for possible copper delamination, the effect of chloride availability [13], and temperature on the completeness of the discharge process. These effects would most likely be able to be captured by the diffusion term when using data from a multi-cell stack where the effects could reasonably be expected to average out over a larger cell count.

With respect to the short-term diffusion cell data, the estimated voltage curves are a much better qualitative fit, following the slope of the true curves to a greater extent. When examining the corresponding underlying concentration trajectories, the estimated concentrations from the short-term diffusion cell data are physically plausible, and Cu^+ clearly accumulates in the catholyte circuit over time as expected due to diffusion and subsequent comproportionation. Furthermore, the estimated membrane diffusion coefficient clearly increases—by roughly a factor of two—due to the ageing process, while all other parameters did not change significantly, which is expected due to membrane degradation. This suggests that the proposed model is capable of meaningfully quantifying the long-term SOH of CuRFBs via the metric proposed in Equation (17).

However, when examining the concentration trajectories from the longer-term cycling data in Figure 11, this is inconsistent with the expected dynamics despite the reasonable-looking voltage fits in Figure 9. In particular, Cu^+ does not appear to accumulate in the catholyte circuit as expected, and the much larger initial concentration of Cu^+ in the anolyte–catholyte circuit is likewise inconsistent with expectations. This discrepancy is most likely attributable to the fact that the current model does not account for the possibility of Cu^+ diffusing from the catholyte to the anolyte through the membrane, in addition to the caveats mentioned concerning the single-cell data.

7. Conclusions

This work has proposed an electrochemical model of the all-copper redox flow battery based exclusively on its three aqueous copper species, as well as a variation in the genetic algorithm to estimate model parameters from experimental data.

The results indicate that the proposed model structure is capable of reproducing experimentally observed voltages to a significant extent while also producing plausible underlying concentration trajectories. However, the results may be significantly degraded if multiple cycles are considered, which the authors consider is likely due to the effects of the unmodelled electrodeposition and electro-stripping dynamics of the solid Cu^0 . The authors do note, however, that the model does produce good estimates on short timescales, appears to accurately predict SOH degradation due to the buildup of excess Cu^+ in the catholyte circuit, and appears to be capable of quantifying longer-term battery degradation via an increase in the estimated membrane diffusion coefficient.

While the proposed model is likely accurate enough to enable SOC estimation based on a scheme such as that proposed in [17], it is also clear that the proposed model represents a first step in the dynamical modelling of all copper-based redox flow batteries, and further refinement is required. We suggest that this refinement should, in particular, be targeted towards clarifying the influence of Cu^0 -related processes on the battery dynamics, as well as clarifying whether said processes can be modelled in a way that is both sufficiently accurate and suitable for control and estimation purposes without compromising on the lumped nature of the proposed model.

Author Contributions: Conceptualisation, C.M.J., W.B. and Z.E.; Investigations, W.B., U.J., C.M.J. and L.M.; Validation, U.J., C.M.J., W.B. and L.M.; Resources, L.M. and W.B.; Writing—original draft preparation, C.M.J., Z.E., U.J., W.B. and L.M.; Writing—review and editing, C.M.J. and W.B.; Visualisation, C.M.J. and W.B.; Supervision, L.M.; Project administration, L.M. All authors have read and agreed to the published version of the manuscript.

Funding: The research leading to these results has been performed within the CuBER project and received funding from the European Community's Horizon 2020 Programme (H2020/2014-2020) under grant agreement #875605.

Data Availability Statement: The data presented in this study are openly available in the following repository: https://github.com/uffejak/cuber_rust_ga (accessed on 17 March 2023), or by request from the corresponding author.

Conflicts of Interest: The authors declare no conflict of interest.

References

1. Ruetschi, P. Energy storage and the environment: The role of battery technology. *J. Power Sources* **1993**, *42*, 1–7. [CrossRef]
2. Ren, M.; Mitchell, C.R.; Mo, W. Managing residential solar photovoltaic-battery systems for grid and life cycle economic and environmental co-benefits under time-of-use rate design. *Resour. Conserv. Recycl.* **2021**, *169*, 105527. [CrossRef]
3. Ahmed, A.; Ge, T.; Peng, J.; Yan, W.C.; Tee, B.T.; You, S. Assessment of the renewable energy generation towards net-zero energy buildings: A review. *Energy Build.* **2022**, *256*, 111755. [CrossRef]
4. Vazquez, S.; Lukic, S.M.; Galvan, E.; Franquelo, L.G.; Carrasco, J.M. Energy storage systems for transport and grid applications. *IEEE Trans. Ind. Electron.* **2010**, *57*, 3881–3895. [CrossRef]
5. Zhang, D.; Liu, Q.; Li, Y. Design of flow battery. In *Reactor and Process Design in Sustainable Energy Technology*; Elsevier: Amsterdam, The Netherlands, 2014; pp. 61–97.
6. Zhang, H.; Li, X.; Zhang, J. *Redox Flow Batteries: Fundamentals and Applications*; CRC Press: Boca Raton, FL, USA, 2017.
7. Ye, R.; Henkensmeier, D.; Yoon, S.J.; Huang, Z.; Kim, D.K.; Chang, Z.; Kim, S.; Chen, R. Redox flow batteries for energy storage: A technology review. *J. Electrochem. Energy Convers. Storage* **2018**, *15*, 010801. [CrossRef]
8. Aluko, A.; Knight, A. A Review on Vanadium Redox Flow Battery Storage Systems for Large-Scale Power Systems Application. *IEEE Access* **2023**, *11*, 13773–13793. [CrossRef]
9. Sanz, L.; Badenhorst, W.D.; Lacarbonara, G.; Faggiano, L.; Lloyd, D.; Kauranen, P.; Arbizzani, C.; Murtomäki, L. All-copper Flow Batteries. In *Flow Batteries*; John Wiley & Sons, Ltd.: Hoboken, NJ, USA, 2023; Chapter 38, pp. 855–873. [CrossRef]
10. Faggiano, L.; Lacarbonara, G.; Badenhorst, W.; Murtomäki, L.; Sanz, L.; Arbizzani, C. Short thermal treatment of carbon felts for copper-based redox flow batteries. *J. Power Sources* **2022**, *520*, 230846. [CrossRef]

11. Sanz, L.; Lloyd, D.; Magdalena, E.; Palma, J.; Kontturi, K. Description and performance of a novel aqueous all-copper redox flow battery. *J. Power Sources* **2014**, *268*, 121–128. [[CrossRef](#)]
12. Zanzola, E.; Gentil, S.; Gschwend, G.; Reynard, D.; Smirnov, E.; Dennison, C.; Girault, H.H.; Peljo, P. Solid electrochemical energy storage for aqueous redox flow batteries: The case of copper hexacyanoferrate. *Electrochim. Acta* **2019**, *321*, 134704. [[CrossRef](#)]
13. Badenhorst, W.D.; Sanz, L.; Arbizzani, C.; Murtoimäki, L. Performance improvements for the all-copper redox flow battery: Membranes, electrodes, and electrolytes. *Energy Rep.* **2022**, *8*, 8690–8700. [[CrossRef](#)]
14. Lloyd, D.; Magdalena, E.; Sanz, L.; Murtoimäki, L.; Kontturi, K. Preparation of a cost-effective, scalable and energy efficient all-copper redox flow battery. *J. Power Sources* **2015**, *292*, 87–94. [[CrossRef](#)]
15. Cruz-Zabalegui, A.; Antaño, R.; Rivera, F. Experimental Evaluation of Copper Redox Couples in Aqueous and Aprotic Electrolytes, for Their Application in A Flow Battery. *Electrochim. Acta* **2023**, *448*, 142189. [[CrossRef](#)]
16. Badrinarayanan, R.; Zhao, J.; Tseng, K.; Skyllas-Kazacos, M. Extended dynamic model for ion diffusion in all-vanadium redox flow battery including the effects of temperature and bulk electrolyte transfer. *J. Power Sources* **2014**, *270*, 576–586. [[CrossRef](#)]
17. Clemente, A.; Montiel, M.; Barreras, F.; Lozano, A.; Costa-Castello, R. Vanadium redox flow battery state of charge estimation using a concentration model and a sliding mode observer. *IEEE Access* **2021**, *9*, 72368–72376. [[CrossRef](#)]
18. Liu, S.; Jiang, J.; Shi, W.; Ma, Z.; Guo, H. Butler–volmer-equation-based electrical model for high-power lithium titanate batteries used in electric vehicles. *IEEE Trans. Ind. Electron.* **2015**, *62*, 7557–7568. [[CrossRef](#)]
19. Bosworth, J.; Foo, N.Y.; Zeigler, B.P. *Comparison of Genetic Algorithms with Conjugate Gradient Methods*; Technical Report; NASA: Washington, DC, USA, 1972.
20. Golub, M. An Implementation of Binary and Floating Point Chromosome Representation in Genetic Algorithm. 1996. Available online: <http://www.zemris.fer.hr/~golub/clanci/iti96.pdf> (accessed on 17 March 2023).
21. Janikow, C.Z.; Michalewicz, Z. An Experimental Comparison of Binary and Floating Point Representations in Genetic Algorithms. In Proceedings of the International Conference on Genetic Algorithms, San Diego, CA, USA, 13–16 July 1991.
22. Kirkpatrick, S.; Gelatt, C.D., Jr.; Vecchi, M.P. Optimization by simulated annealing. *science* **1983**, *220*, 671–680. [[CrossRef](#)] [[PubMed](#)]
23. CuBER Parameter Estimation in Rust. Available online: https://github.com/uffejak/cuber_rust_ga (accessed on 12 March 2023).
24. Kuldeep; Manzanares, J.A.; Kauranen, P.; Mousavihashemi, S.; Murtoimäki, L. Determination of Ionic Diffusion Coefficients in Ion-Exchange Membranes: Strong Electrolytes and Sulfates with Dissociation Equilibria. *ChemElectroChem* **2022**, *9*, e202200403.
25. Krzewska, S. Impedance investigation of the mechanism of copper electrodeposition from acidic perchlorate electrolyte. *Electrochim. Acta* **1997**, *42*, 3531–3540. [[CrossRef](#)]

Disclaimer/Publisher’s Note: The statements, opinions and data contained in all publications are solely those of the individual author(s) and contributor(s) and not of MDPI and/or the editor(s). MDPI and/or the editor(s) disclaim responsibility for any injury to people or property resulting from any ideas, methods, instructions or products referred to in the content.